



A Paper-Supported Photoelectrochemical Sensing Platform Based on Surface Plasmon Resonance Enhancement for Real-Time H₂S Determination

Fang Wang² · Qingfu Fan^{1,3} · Yanhu Wang¹ · Shenguang Ge⁴ · Mei Yan¹ · Jinghua Yu¹

Received: 11 September 2018 / Revised: 20 October 2018 / Accepted: 22 October 2018 / Published online: 2 November 2018
© The Nonferrous Metals Society of China 2018

Abstract

Based on in situ generation of CdS quantum dots (QDs) and surface plasmon resonance (SPR) enhancement between CdS QDs and Ag nanoparticles (NPs), an innovative paper-supported photoelectrochemical (PEC) sensing platform was constructed for real-time intracellular H₂S detection. SiO₂ shell was coated on the Ag NPs to improve the stability of Ag NPs. H₂S was used to trigger the formation of CdS QDs, thereby inducing an improvement of photocurrent response. CdS QDs grown on the Ag@SiO₂ core–shell NPs worked efficiently to absorb visible light. The resulting CdS QDs–Ag@SiO₂ core–shell NPs exhibit improved PEC behavior, which was attributed to the surface plasmon-resonance effect of Ag NPs. Meanwhile, the separation of cell binding from the photoelectrode would eliminate the commonly existing affection during the biorecognition processes. This novel SPR-enhanced PEC sensing platform not only achieved satisfactory analysis results toward H₂S, but also showed excellent sensitivity, selectivity, low cost, and portable features. The strategy of the SPR through the in situ generation of semiconductor nanoparticles on the surface of noble metal semiconductor paves way for the improvements of PEC analytical performance.

Keywords Paper · Photoelectrochemical · Surface plasmon resonance · Ag@SiO₂ · CdS · Intracellular H₂S

Electronic supplementary material The online version of this article (<https://doi.org/10.1007/s41664-018-0070-8>) contains supplementary material, which is available to authorized users.

✉ Yanhu Wang
wyhlloving633@163.com

✉ Jinghua Yu
ujn.yujh@gmail.com

¹ School of Chemistry and Chemical Engineering, University of Jinan, Jinan 250022, People's Republic of China

² School of Biological Science and Technology, University of Jinan, Jinan 250022, People's Republic of China

³ Shandong Provincial Key Laboratory of Preparation and Measurement of Building Materials, University of Jinan, Jinan 250022, People's Republic of China

⁴ Institute for Advanced Interdisciplinary Research, University of Jinan, Jinan 250022, People's Republic of China

1 Introduction

Real-time detection of trace physiologic messenger molecules from cells and tissues is significant for studying fundamental cellular functions researches, disease diagnoses and medical treatments [1, 2]. As the third endogenously generated gaseous signal compound with cytoprotective properties (the other two are nitric oxide and carbon monoxide), hydrogen sulfide (H₂S) has attracted great attention for its recently established function as a signal transmitter in living organisms [3–5]. H₂S was also known to be involved in a variety of physiological processes, such as antioxidation, anti-inflammation, and apoptosis [6–8]. Moreover, the abnormal H₂S level in cells has been associated with various diseases such as Alzheimer's disease, Down's syndrome, diabetes, and liver cirrhosis [9–11]. Accordingly, the development of efficient methods for detection of H₂S in living systems is of considerable significance for better understanding of its physiological and pathological functions and has become one of the most important subjects of current chemical research [12].

Till now, a considerable number of protocols have been focused on the exploration of new approaches for H₂S detection, such as fluorescence, colorimetric and electrochemical analysis [9, 13, 14]. However, those methods are often limited by poor compatibility with live cells, temporal resolution, or extensive sample preparation requirements, which are not appropriate for in situ detection. Photoelectrochemical (PEC) with both advantages of optical and electrochemical methods, have attracted extensive research and undergoes rapid development in recent years [15–19]. As the basis of future sustainable technology, growing interests have led to a number of works on paper-based analytical devices (PADs) due to its low cost, light weight, biodegradability, and biocompatibility [20, 21]. Furthermore, PEC sensing methods have been introduced into PADs to partially circumvent the limitations of traditional PEC systems, which provide access to point-of-care testing in the field of home health-care settings and for implementation in resource limited regions [22–24].

For sensitive PEC sensing platform construction, eminent photoactive materials are of great desired [16]. And quantum dots (QDs) have been adopted as photoactive materials for desired PEC biosensors constructing [22, 25–29]. However, most of the reported PEC sensing platforms adopted pre-synthesized semiconductors as a signal transducer that exhibit several drawbacks, such as high background signals, low sensitivity, time-consuming and increased cost which is unfavorable for PEC detection and in situ monitoring [30]. Luckily, we demonstrated a PEC platform based on in situ generation of CdS QDs through the reaction between S²⁻ and Cd²⁺ makes it possible to break the referred bottlenecks. Nonetheless, the severe recombination rate of photogenerated electron–hole pairs of CdS QDs leads to relatively low light-to-electricity conversion efficiency [31]. To promote the photoelectric conversion efficiency of CdS QDs, surface plasmon resonance (SPR) was introduced, which could transfer the plasmonic energy from the metal to the semiconductor results in efficient generation of electron–hole pairs in semiconductors and hence offers an approach to enhance energy conversion efficiency in PEC processes [32, 33]. Among noble metal nanoparticles (NPs), such as Au, Ag or Pt, Ag NPs has been proven to be one of the most promising noble metals investigated for strong plasmon resonance and high energy conversion efficiency [34]. Nevertheless, the active chemical activity and easily susceptible to surroundings of Ag NPs are not desired [35]. To overcome above disadvantage, a passive, insulating, and optically transparent SiO₂ shell (about 2 nm) was coated on the surface of Ag NPs to improve the stability of Ag NPs.

Herein, we reported a paper-supported PEC sensing platform for real-time intracellular H₂S analysis based on the in situ generation of CdS QDs and SPR enhancement. CdS QDs were generated through the reaction

between S²⁻ and Cd²⁺. The attachment of CdS QDs to Ag@SiO₂ core–shell NPs offers strong SPR enhancement for photo-to-current conversion efficiency. This proposed SPR-enhanced PEC sensing platform demonstrated a new exciting avenue for bioanalysis, and served as guidance for the rational construction of a highly efficient PEC sensing platform.

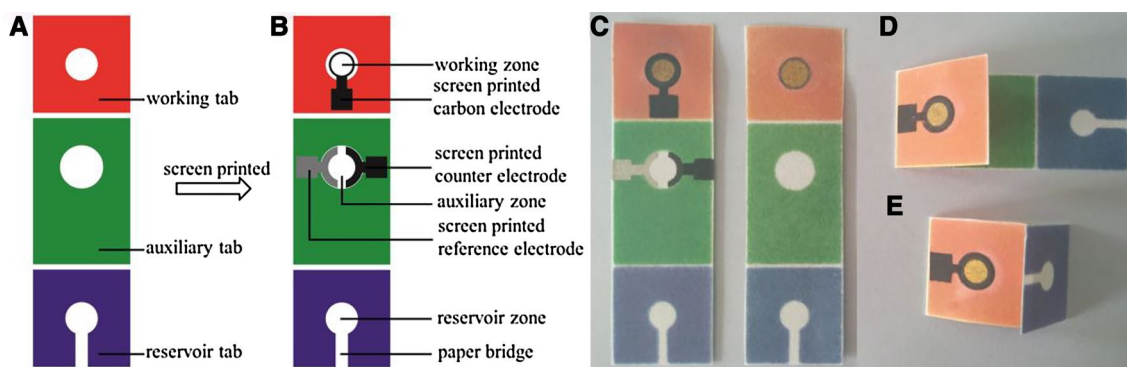
2 Experimental Section

2.1 Materials and Reagents

Silver nitrate (AgNO₃), tetraethyl orthosilicate (TEOS), ethanol, polyvinylpyrrolidone (PVP, *M_w* = 58 000), aqueous ammonia and ethylene glycol were of analytical grade and purchased from Shanghai Chemical Corp. Tetradecanedioic acid (DDCA) was purchased from Adamas Reagent Co. Ltd. Ascorbic acid (AA, ≥ 99.0%), N-19 hydroxysuccinimide (NHS), 1-ethyl-3-(3-dimethylaminopropyl) carbodiimide (EDC) and vascular endothelial growth factor (VEGF) were purchased from Sigma. Indium tin oxide substrates (ITO, a thickness of ITO layer of 150 nm and resistance of 10 Ω·cm⁻²; thickness of glass: 1.1 mm) was obtained from Xiamen ITO Photoelectricity Industry (Xiamen, China). All chemicals were used as received. Ultrapure water (18 MΩ·cm⁻¹) was used for all experiments. The human liver cancer cells HEP G2 cells were provided by Shandong Tumor Hospital.

2.2 Design and Fabrication of PADs

For the preparation of the PADs, wax was used as the paper hydrophobization to construct hydrophobic barrier on paper. Three layers of patterned rectangular papers named as working tab (18.0 mm × 18.0 mm, the red one), auxiliary tab (18.0 mm × 27.0 mm, the green one), and reservoir tab (18.0 mm × 18.0 mm, the blue one) below made up the PADs (Scheme 1a). Only a wax-patterned circular hydrophilic zone (6.0 mm in diameter on working tab, 8.0 mm in diameter on auxiliary tab, 6.0 mm in diameter on reservoir tab) on both tabs. And a paper bridge on the reservoir tab (6.0 mm × 2.0 mm) was used to connect the hydrophilic zones on working tab and reservoir tab after folding. After baking the wax-patterned paper sheet in an oven at 130 °C for 150 s, the as-prepared sheet was ready for printing electrode after cooling to room temperature. The screen-printing carbon electrode was screen-printed onto the patterned working zone of working tabs, the carbon counter electrode and Ag/AgCl reference electrode were screen-printed onto reference zone of auxiliary tabs (Scheme 1b).



Scheme 1 Schematic representation of the PAD. **a** Wax patterns of this PAD; **b** the PAD after screen-printing; **c** picture of this PAD, front side (left) and reverse side (right); assay procedures of this

PAD: **d** the working tab was folded above the auxiliary tab; **e** the reservoir tab was folded above the working tab

2.3 Synthesis of Ag NPs

Ag NPs with an average size of about 60 nm in diameter were synthesized according to the previous method with modification [35]. In a typical synthesis procedure, 15 mM of AgNO_3 and 100 mM of PVP ($M_w = 58\,000$) dissolved in 20 mL of ethylene glycol were mixed under vigorous stirring. Then the mixture was heated to 130 °C and kept for 1 h without further stirring. After that, 100 mL acetone was added to the mixture solution under sonication, followed by incubation for 30 min. The sediment containing Ag NPs was separated from the mixture solution under centrifugation at 8500 rpm for 10 min. The obtained precipitates were washed with ethanol and ultrapure water thrice, and redispersed in 10 mL of ethanol to obtain the 0.02 g mL^{-1} of Ag NPs/ethanol solution.

2.4 Synthesis of Ag@SiO₂ Core–Shell NPs

In order to improve the stability and reduce the intrinsic toxicity of silver, a thin silica layer coated on the surface of obtained Ag NPs was prepared [36]. Briefly, 2 mL of above obtained Ag NPs/ethanol solution was added into 15 mL of anhydrous ethanol and gently stirred for 30 min at room temperature, subsequently 10 mL deionized water and 0.5 mL ammonia aqueous solution (28 wt%) were added into the mixture, and the mixture was stirred for another 5 min. Then 20 μL of TEOS in anhydrous ethanol (10 mM) were introduced drop by drop with continuous stirring, and the reaction was continued for 12 h. The suspension of Ag@SiO₂ core–shell NPs was centrifuged at 7000 rpm for 10 min and washed with ultrapure water and ethanol for 3 times and redispersed in 10 mL of ethanol. For the Cd^{2+} absorption, the obtained product was mixed with 10 mL 100 mM CdSO_4 . After stirring the solution for 6 h at room temperature, the products were isolated by centrifugation and rinsed with ultrapure water to remove excess ions that were weakly

bounded to the Ag@SiO₂ core–shell NPs surfaces. Finally, the precipitate was redispersed in 5 mL ultrapure water for future use. Bare SiO₂ NPs was prepared without the addition of Ag NPs.

2.5 Cell Culture

HEP G2 (human liver carcinoma) cells were kindly provided by Shandong Tumor Hospital. HEP G2 cells were cultured and maintained in exponential growth in RPMI 1640 medium (GIBCO) containing 10% fetal calf serum (HyClone, Logan, UT), penicillin (100 units mL^{-1}), and streptomycin (100 $\mu\text{g}\cdot\text{mL}^{-1}$) at 37 °C in a humidified incubator containing 5% CO₂. HEP G2 cells were separated from the medium by centrifugation at 1000 rpm for 5 min, and then washed thrice with 0.01 M PBS (pH 7.4). The supernatant was aspirated, and the cells were re-suspended in incubation buffer (4.5 g/L glucose, 5.0 mM MgCl_2 , 0.1 mg/mL tRNA, and 1 mg/mL BSA, all dissolved in Dulbecco's PBS with CaCl_2 and MgCl_2) to obtain a homogeneous cell suspension at a certain concentration. The incubation buffer was used to ensure the effective binding affinity between cells and the aptamer. Cell number was determined using a Petroff–Hausser cell counter (USA).

2.6 CdS QD-Mediated Determination of S²⁻

An interconnected Au NPs layer was first grown on the cellulose fibers of paper working electrode (PWE) (Scheme 1c). Briefly, 12 nm Au NPs seeds were prepared using sodium citrate as reductant. Then, 15.0 μL as-prepared Au NP seeds solution were dropped into the paper sample zone of bare PWE, kept at room temperature for 1 h for Au NP seeds immobilization. Loosely bound Au NP seeds were removed through rinsing, then 15 μL freshly prepared growth aqueous solution of 10 mM PBS (pH 7.0) containing 1.2 mM HAuCl_4 , 2.0 mM cetyltrimethylammonium chloride and

7.2 mM H_2O_2 for seeds growth were applied into the Au NP-seeded PWE, and incubated at room temperature for 10 min. Subsequently, the resulting porous Au–PWE was washed with water thoroughly. Finally, a layer of interconnected Au NPs on cellulose fibers with good conductivity were obtained.

A 20 μL solution of Cd^{2+} -doped Ag@SiO_2 was dropped onto the surface of Au–PWE, dried at room temperature, and rinsing with ultrapure water. After that, 20 μL Na_2S aqueous solution with different concentration was added onto the modified Au–PWE and incubated for 10 min, followed by washing with PBS solution (0.01 M, pH 7.4) thoroughly to remove excess S^{2-} drying at room temperature. And the working tab was flopped over on the auxiliary tab (Scheme 1d). Photoelectrochemical detection was performed at room temperature with dropping 20 μL PBS (pH 7.4, 0.1 M) including 0.1 M ascorbic acid (AA) as a sacrificial electron donor into Au–PWE during measurement of the photocurrent. Visible light generated by a xenon lamp was employed as excitation light source. The applied voltage was 0.0 V.

2.7 Determination of H_2S Released from HEP G2 Cell

To demonstrate the sensitivity of the PEC transducer to H_2S released from HEP G2 cells, a certain amount of HEP G2 cells were added onto the reservoir zone on reservoir tab. And then 20 μL of 35 $\text{ng}\cdot\text{mL}^{-1}$ vascular endothelial growth factor (VEGF) was added and kept 30 min to stimulate HEP G2 cells releasing H_2S . After that, working tab was flopped over on the auxiliary tab, and the reservoir tab was followed flopped over on the working tab (Scheme 1e). With the addition of 30 μL PBS to the hydrophilic circler zone on reservoir tab, the generated H_2S was transferred to the working zone via the paper bridge. After 10 min reaction, the reservoir tab was unfolded, and the working zone was rinsed with water. Then the PEC detection was carried out under the visible light irradiation at a constant potential of 0 V with the introduction of 20 μL AA (0.1 M), which was deaerated by highly pure nitrogen prior to measurements.

3 Results and Discussion

3.1 Materials Characterization

Figure S1 in ESI shows the TEM image of the Ag NPs; irregular spherical with the size distribution about 60 nm which provided the highest enhancement factor were observed [34]. Due to the instability of pure Ag NPs, the morphology of Ag NPs changed easily, and the size is not very uniform. Figure 1a exhibits the TEM image of bare SiO_2 sphere with the diameter around 60 nm. Figure 1b shows TEM images of the well-dispersed core/shell type Ag@SiO_2 NPs. Apparently, uniform SiO_2 shells with uniform thickness were coated onto Ag NPs beads. Compared with SiO_2 sphere, a clear core could be seen. TEM images in Fig. 1c provided direct evidence for the formation of CdS QDs on the surface of Ag@SiO_2 core–shell NPs. Compared with bare Ag@SiO_2 core–shell NPs shown in Fig. 1b, it could be clearly seen that small nanoparticles are homogeneously and densely dispersed onto the surfaces of Ag@SiO_2 core–shell NPs with closely contacted interfaces. Furthermore, from Fig. 1c, we could see that amounts of black dots uniformly decorated on the surface of Ag@SiO_2 core–shell NPs. In addition, the existence of CdS in the composite is directly confirmed through the measure lattice spacing corresponding to the CdS (002) planes (inset in Fig. 3c). High-resolution TEM image while that of 0.34 nm in the CdS coating region is in accordance with the spacing of (002) planes of wurtzite CdS successfully demonstrated the formation of CdS.

Optical properties of the prepared samples were tested using UV–Vis diffuse reflectance spectroscopy. Figure 2a shows the UV–Vis diffuse reflectance spectra of Ag NPs, Ag@SiO_2 core–shell NPs and CdS– Ag@SiO_2 core–shell NPs. Compared to the absorption spectrum of Ag NPs in aqueous solution (curve a), the formation of Ag@SiO_2 core–shell NPs accompanied with absorption red shift (curve b). The red shift from 420 to 450 nm is attributed to the progressive formation of SiO_2 shell upon the Ag NPs. This peak shift may have been caused by the dielectric variance of shape and dielectric environment of the nanoparticles [37]. The absorption spectra revealed that SiO_2 shell

Fig. 1 TEM images of SiO_2 (a), Ag@SiO_2 core–shell NPs (b) and CdS– Ag@SiO_2 core–shell NPs (c), inset is the HRTEM image of CdS

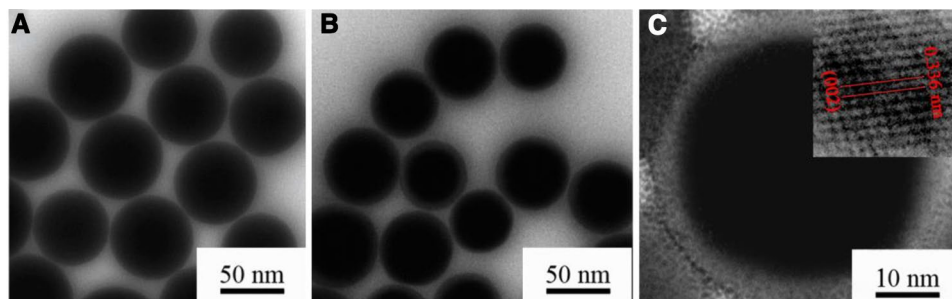


Fig. 2 UV–Vis diffuse reflectance spectroscopy (a) and XRD patterns (b) of Ag NPs (curve a), Ag@SiO₂ core–shell NPs (curve b) and CdS–Ag@SiO₂ core–shell NPs (curve c)

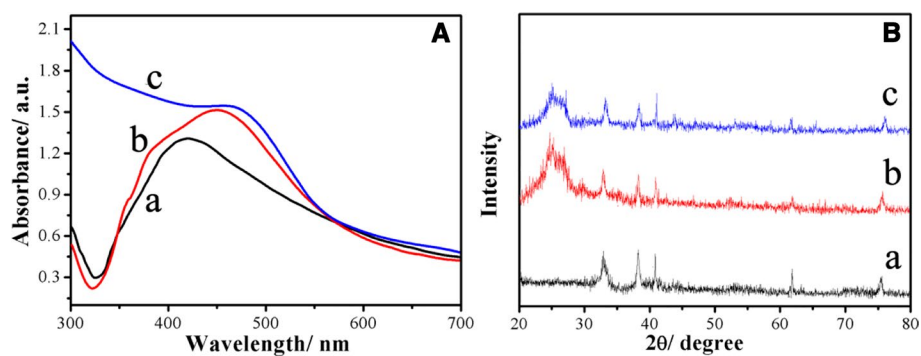
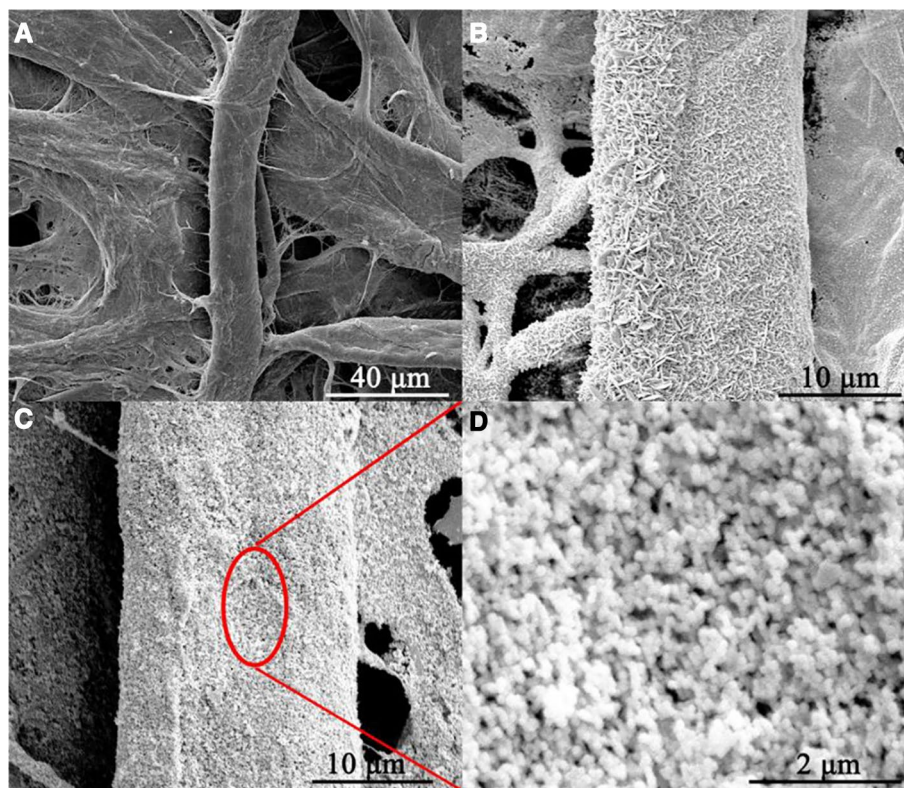


Fig. 3 SEM of bare fibers (a), Au–PWE (b), and Cd²⁺-doped Ag@SiO₂ decorated Au–PWE (c, d)



was successfully attached to the surface of the Ag NPs array. A remarkable red shift was observed after formation of CdS–Ag@SiO₂ core–shell NPs (curve c), which could be attributed to the absorption of the generated CdS nanoparticles. The X-ray diffraction (XRD) patterns of Ag NPs, Ag@SiO₂ core–shell NPs and CdS–Ag@SiO₂ core–shell NPs are displayed in Fig. 2b. According to the XRD of the as-prepared Ag NPs (curve a), four peaks located at 38.0°, 44.4°, 64.4°, and 77.3° are assigned to (111), (200), (220), and (311) faces of a Ag crystal, respectively, demonstrating the formation of metallic Ag NPs [38]. After the formation of Ag@SiO₂ core–shell NPs, a typical unformed SiO₂ peak around 22° was observed that demonstrated the presence of SiO₂ (curve b). No additional diffraction peaks were observed in the CdS–Ag@SiO₂ core–shell NPs (curve c),

which was presumably due to the relatively low incorporation and small size of the CdS.

3.2 Characterization of PWE

It was observed that the porous bare paper possessed high surface area with rough cellulose surface which could provide an excellent adsorption microenvironment further modification (Fig. 3a). After Au NPs growth, a compact layer of Au NPs assembled onto the surfaces of interwoven cellulose which would greatly promote the conductivity (Fig. 3b). Then, Cd²⁺-doped Ag@SiO₂ were connected to the surface of the Au–PWE (Fig. 3c, d) to greatly increase the active surface area.

3.3 Plasmon-Enhanced Photocurrent Response and Mechanism

The fabrication of the PEC transducer could be monitored by corresponding photocurrent measurements. Figure 4 shows the photocurrent generated under visible light irradiation. The photocurrent response appeared immediately upon irradiation and fell down instantly when the irradiation was cut off. There was no photocurrent response for Au–PWE (curve a). The photocurrent increased significantly when the Cd^{2+} -doped Ag@SiO_2 core–shell NPs were casted onto the Au–PWE (curves b), which was attributed to SPR-mediated hot electrons transfer (ET) from metal to electrode [39]. The generated photocurrent further improved with the increased concentration of S^{2-} (curve c to e), that could be used for S^{2-} recording. This improvement was attributed to the formation of CdS QDs in the presence of S^{2-} or H_2S (Scheme 2, as formula 1 described). While, after immobilization of Cd^{2+} -doped SiO_2 NPs, no obvious photocurrent change could be observed (curve g). More interestingly, compared with the 100 nM S^{2-} treated Cd^{2+} -doped Ag@SiO_2 core–shell NPs (curve d), the photocurrent generated from 100 nM S^{2-} treated the Cd^{2+} -doped SiO_2 NPs (curve f) is lower. All those demonstrated that the enhancement of photocurrent was ascribed to the formation of CdS and SPR effect,



Based on the results above, the major mechanism responsible for the improved PEC performance is believed to be

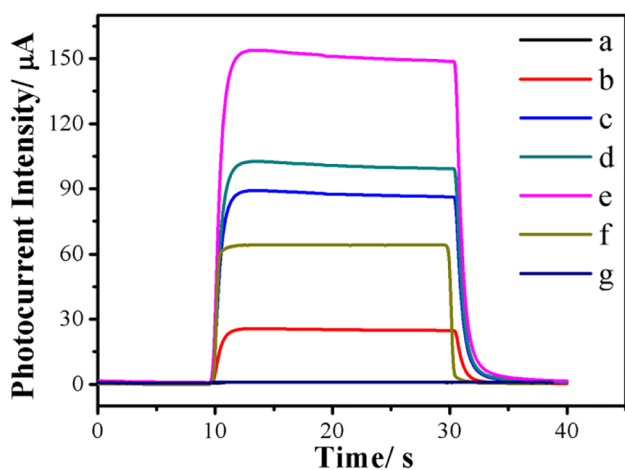
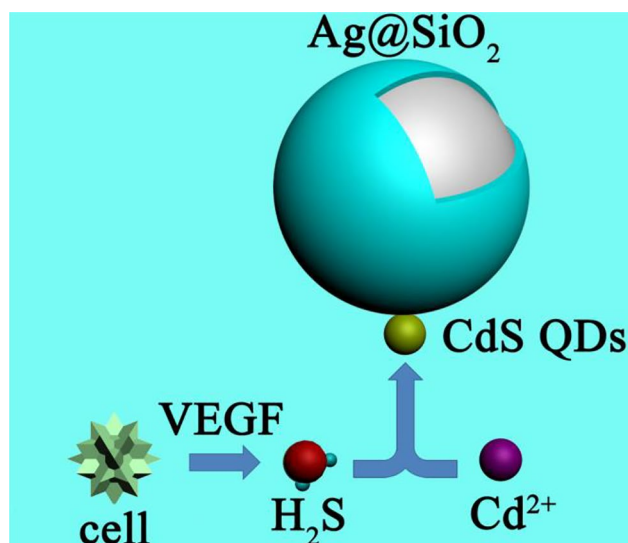
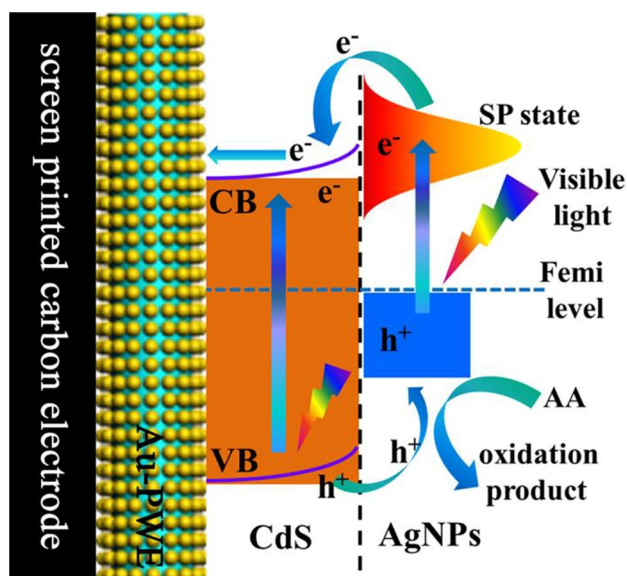


Fig. 4 Photocurrent response of different photoelectrodes: Au–PWE (a); Cd^{2+} -doped Ag@SiO_2 core–shell NPs modified Au–PWE (b); Cd^{2+} -doped Ag@SiO_2 core–shell NPs reacted with different concentrations of S^{2-} (curve c, d, e, 10 nM, 100 nM and 1 μM , respectively); Cd^{2+} -doped SiO_2 NPs modified Au–PWE treated with 100 nm S^{2-} (f); and Cd^{2+} -doped SiO_2 NPs modified Au–PWE (g)



Scheme 2 Schematic H_2S release and generation of CdS QDs on Ag@SiO_2 for the detection of S^{2-}

the hot electron-transfer mechanism and CdS generation. As presented in Scheme 3, under visible light illumination, photoelectrons generated from valence band (VB) migrated to the conduction band (CB) of CdS QDs. Meanwhile, the Ag NPs absorbed plasmon-induced irradiation, and then generated hot electrons and an electromagnetic field. The plasmon-induced hot electrons were injected into the CB of CdS QDs over the Schottky barrier which could promote charge separation and interfacial photoinduced holes transmission, and eventually enhanced the photocurrent [40]. Finally, the



Scheme 3 Schematic illustration of mechanism of explaining the enhanced PEC performance

photoelectrons were transferred to the Au–PWE generating photocurrent that could be recorded by the electrochemical workstation. Meanwhile, the left holes in the VB of CdS migrated to Ag NPs, facilitating the generation of photoelectrons by photoexcitation [41]. AA was used as sacrificial reagent, which scavenged the generated holes locating on excited state of Ag NPs. All those could improve the PEC performance and resulted in improvement of PEC detection sensitivity.

3.4 Cell Viability and MTT Assay

To inspect whether the prepared materials affect the cell viability, a standard staining method was adapted by the use of the calcein-AM. The cytotoxicity test of the Cd²⁺-doped Ag@SiO₂ core–shell NPs was performed, HEP G2 cancer cells were incubated with Cd²⁺-doped Ag@SiO₂ core–shell NPs for 4 h, Media in the dishes were discarded and the cells were separated followed by gently rinsing with PBS. 1 mL of the calcein-AM was added into the dishes and incubated for 15 min at 37 °C. As shown in Fig. 5a, Cd²⁺-doped Ag@SiO₂ core–shell NPs have no apparent effect on cancer cells within 30 min.

Biocompatibility is also considered as one of the foremost properties for a probe to be practically used in living cells. The cytotoxicity of Cd²⁺-doped Ag@SiO₂ core–shell NPs on HEP G2 cells was evaluated by a standard 3-(4,

5-dimethyl-2-thiazolyl)-2,5-diphenyltetrazolium bromide (MTT) assay according to previous work [42]. No apparent effects on the cell viability with the extending of incubation time within 30 min (Fig. 5b). It should be noticeable that the viability of the cells decreased obviously with the incubation time extended which might be attributed to the toxicity of Cd²⁺. However, the quantitative determination of H₂S released from HEP G2 Cells, the separation of the Cd²⁺-doped Ag@SiO₂ core–shell NPs and HEP G2 Cells and the optimal incubation time (30 min) would also be favorable to guarantee the cell viability.

3.5 Analytical Performance

The photocurrent intensity of the prepared PEC sensing platform is effectively enhanced by trace amounts of S²⁻, demonstrating its potential for S²⁻ determination. Figure 6a presents the effect of various concentrations of S²⁻ on the photocurrent intensity of the prepared PEC biosensor under the optimum condition (Figure S2). Clearly, the photocurrent intensity increased with the increase of S²⁻ concentration. And the photocurrent was proportional to the logarithm value of S²⁻ concentration in the range from 1.0 nM to 5 mM with a correlation equation of $I = 43.591 \text{ gC}(\text{nM}) + 28.73$ ($R = 0.9935$), whereas I was the photocurrent intensity and C was the S²⁻ concentration (Fig. 6b). The detection limit of S²⁻ was calculated to

Fig. 5 **a** Fluorescence imaging of the HEP G2 cancer cells after the incubation with Cd²⁺-doped Ag@SiO₂ core–shell NPs for 30 min. **b** Cytotoxicity of Cd²⁺-doped Ag@SiO₂ core–shell NPs on HEP G2 cells determined by MTT assay

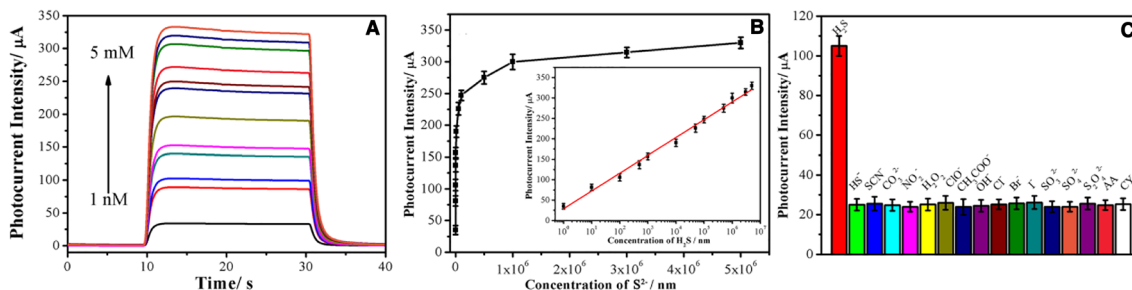
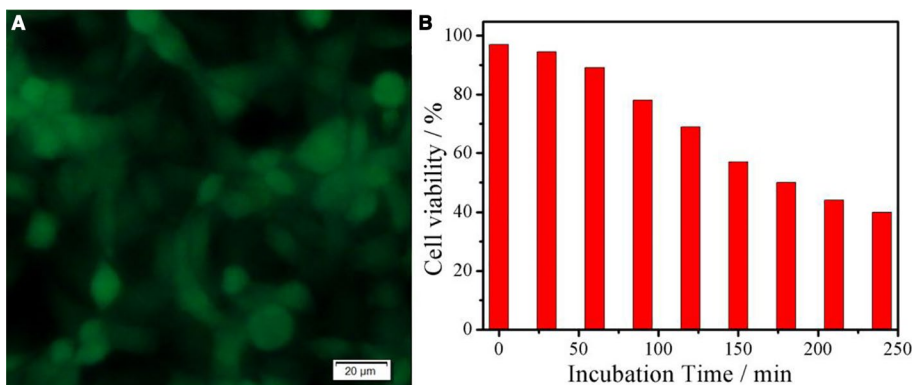


Fig. 6 **a** Photocurrent responses of the proposed method towards different S²⁻; **b** calibration curve for determination of S²⁻; **c** selectivity of the proposed PEC sensing platform

be $0.37 \text{ ng}\cdot\text{mL}^{-1}$ ($S/N=3$). Compared with other methods reported in the literatures (Table 1), this work had a relative large linear range and low detection limit. In addition, the proposed method exhibits potential for detection of S^{2-} in the subnanomolar level. The excellent sensitivity of this PEC strategy might be attributed to the high photovoltaic conversion efficiency and the reliable stability of the formed CdS QDs and Ag@SiO₂ core-shell NPs.

To evaluate the selectivity of the designed strategy for S^{2-} assay, the photocurrent response of this system was investigated against other common analogues including HS^- , SCN^- , CO_3^{2-} , NO_2^- , H_2O_2 , ClO^- , CH_3COO^- , OH^- , Cl^- , Br^- , I^- , SO_3^{2-} , $\text{S}_2\text{O}_3^{2-}$, SO_4^{2-} , $\text{S}_2\text{O}_4^{2-}$, ascorbic acid (AA), and cysteine (CY). As shown in Fig. 6c, no significant photocurrent change was observed upon the addition of tenfold excess of other interfering ions in comparison with S^{2-} . All these results demonstrated that the PEC probe is highly selective for S^{2-} over other biological related species and could meet the selective requirements.

3.6 Analysis of H₂S Released from HEP G2 Cells

To determine whether our presented method could respond to intracellular H₂S, HEP G2 cell was chosen as the model cancer cell, while VEGF was used as the stimulant agent, which will induce the H₂S generation from cancer cells with consistent photocurrent response. When the cancer cells were stimulated, larger amount of H₂S releasing occurred. The photocurrent intensity reached to 294 μA after the incubation of 1×10^4 cells/mL, corresponding to the concentration of H₂S released from single cancer cell about 1.23×10^{-7} mol. This value matches well with the previous reports [46], all those demonstrated a satisfactory analytical performance of the as-prepared PEC sensing platform and validated the feasibility of the proposed strategy.

Table 1 Comparison of analytical properties of different methods toward S^{2-}

Methods	Linear range (μM)	Detection limit (nM)	References
Fluorescence	0–10	250	[3]
Colorimetric	0–2	7	[13]
Colorimetric	0–10	300	[43]
Fluorescence	0–100	–	[44]
Photoelectrochemical	0.01–1000	0.7	[45]
Photoelectrochemical	10^{-3} –1000	0.37	This work

4 Conclusions

In summary, we have developed a paper-supported SPR-enhanced PEC sensing platform by in situ generation of CdS QDs on Ag@SiO₂ core-shell NPs for real-time analysis of H₂S in living cells. The in situ generation of CdS QDs offers a green and efficient alternative to inconvenient presynthesis procedures for the fabrication of semiconducting nanoparticles. In addition, the close proximity of CdS QDs and Ag NPs provides a strong SPR effect promotes charges separation and interfacial photoinduced electron transmission as well as reduces the electron-hole recombination thus significantly enhance the photocurrent. Moreover, the proposed PEC sensing platform also exhibits a wide linear response range, low detection limit and good reproducibility in the assay of H₂S, thus not only provides a new strategy for designing a low-cost and sensitive PEC dynamic sensing interface toward living cells, but also can be extended to detect other important biomolecules and has a wide potential application in bioanalysis.

Acknowledgements This work was financially supported by the program for Taishan Scholar of Shandong Province (ts201712048) and National Natural Science Foundation of China (21874055, 51632003). Supports from the 111 Project of International Corporation on Advanced Cement-based Materials (No. D17001) is greatly appreciated.

References

- Lin VS, Lippert AR, Chang CJ. Cell-trappable fluorescent probes for endogenous hydrogen sulfide signaling and imaging H₂O₂-dependent H₂S production. *Proc Natl Acad Sci USA*. 2013;110:7131–5.
- Jie X, Yang H, Wang M, Zhang Y, Wei W, Xia Z. A Peroxisome-inspired chemiluminescent silica nanodevice for the intracellular detection of biomarkers and its application to insulin-sensitizer screening. *Angew Chem Int Ed*. 2017;129(46):14788–93.
- Karakus E, Ucuncu M, Emrullahoglu M. Electrophilic cyanate as a recognition motif for reactive sulfur species: selective fluorescence detection of H₂S. *Anal Chem*. 2016;88:1039–43.
- Gao Z, Tang D, Tang D, Niessner R, Knopp D. Target-induced nanocatalyst deactivation facilitated by core@shell nanostructures for signal-amplified headspace-colorimetric assay of dissolved hydrogen sulfide. *Anal Chem*. 2015;87(19):10153–60.
- Zhang Z, Chen Z, Wang S, Qu C, Chen LX. On-site visual detection of hydrogen sulfide in air based on enhancing the stability of gold nanoparticles. *ACS Appl Mater Interfaces*. 2014;6(9):6300–7.
- Kong H, Ma Z, Wang S, Gong X, Zhang S, Zhang X. Hydrogen sulfide detection based on reflection: from a poison test approach of ancient China to single-cell accurate localization. *Anal Chem*. 2014;86(15):7734–9.
- Tang J, Zhang Y, Kong B, Wang Y, Da P, Li J, Elzatahry AA, Zhao D, Gong X, Zheng G. Solar-driven photoelectrochemical probing of nanodot/nanowire/cell interface. *Nano Lett*. 2014;14(5):2702–8.

8. Omar Yassine OS, Assen H, Belmabkhout Y, Salama KN, Eddaoudi M. H₂S sensors: fumarate-based fcu-MOF thin film grown on a capacitive interdigitated electrode. *Angew Chem Int Ed.* 2016;55(51):15879–83.
9. Peng H, Cheng Y, Dai C, King AL, Predmore BL, Lefer DJ, Wang B. A fluorescent probe for fast and quantitative detection of hydrogen sulfide in blood. *Angew Chem Int Ed.* 2011;50(41):9672–5.
10. Hao J, Xiong B, Cheng X, He Y, Yeung ES. High-throughput sulfide sensing with colorimetric analysis of single Au–Ag core-shell nanoparticles. *Anal Chem.* 2014;86(10):4663–7.
11. Bailey TS, Pluth MD. Chemiluminescent detection of enzymatically produced hydrogen sulfide: substrate hydrogen bonding influences selectivity for H₂S over biological thiols. *J Am Chem Soc.* 2013;135(44):16697–704.
12. Yu Q, Zhang KY, Liang H, Zhao Q, Yang T, Liu S, Zhang C, Shi Z, Xu W, Huang W. Dual-emissive nanohybrid for ratiometric luminescence and lifetime imaging of intracellular hydrogen sulfide. *ACS Appl Mater Interfaces.* 2015;7(9):5462–70.
13. Yan Y, Yu H, Zhang Y, Zhang K, Zhu H, Yu T, Jiang H, Wang S. Molecularly engineered quantum dots for visualization of hydrogen sulfide. *ACS Appl Mater Interfaces.* 2015;7(6):3547–53.
14. Xu T, Scafa N, Xu LP, Zhou S, Abdullah Al-Ghanem K, Mahboob S, Fugetsu B, Zhang X. Electrochemical hydrogen sulfide biosensors. *Analyst.* 2016;141(4):1185–95.
15. Zhao W, Xu JJ, Chen HY. Photoelectrochemical DNA biosensors. *Chem Rev.* 2014;114(15):7421–41.
16. Wang Y, Shi H, Cui K, Zhang L, Ge S, Yan M, Yu J. Hierarchical hematite/TiO₂ nanorod arrays coupled with responsive mesoporous silica nanomaterial for highly sensitive photoelectrochemical sensing. *Biosens Bioelectron.* 2018;117:515–21.
17. Wang Y, Zhang L, Cui K, Xu C, Li H, Liu H, Yu J. Solar driven electrochromic photoelectrochemical fuel cells for simultaneous energy conversion, storage and self-powered sensing. *Nanoscale.* 2018;10(7):3421–8.
18. Wang YH, Ge SG, Zhang L, Yu JH, Yan M, Huang JD. Visible photoelectrochemical sensing platform by in situ generated CdS quantum dots decorated branched-TiO₂ nanorods equipped with Prussian blue electrochromic display. *Biosens Bioelectron.* 2017;89:859–65.
19. Li H, Li J, Zhu Y, Xie W, Shao R, Yao X, Gao A, Yin YD. Cd²⁺-doped amorphous TiO₂ hollow spheres for robust and ultrasensitive photoelectrochemical sensing of hydrogen sulfide. *Anal Chem.* 2018;90(8):5496–502.
20. Kentaro Yamada TGH, Suzuki K, Citterio D. Paper-based inkjet-printed microfluidic analytical devices. *Angew Chem Int Ed.* 2015;54(18):5294–310.
21. Yang H, Zhang Y, Zhang L, Cui K, Ge S, Huang J, Yu J. Stackable lab-on-paper device with all-in-one Au electrode for high-efficiency photoelectrochemical cyto-sensing. *Anal Chem.* 2018;90(12):7212–20.
22. Wang Y, Ge L, Wang P, Yan M, Ge S, Li N, Yu J, Huang J. Photoelectrochemical lab-on-paper device equipped with a porous Au-paper electrode and fluidic delay-switch for sensitive detection of DNA hybridization. *Lab Chip.* 2013;13(19):3945–55.
23. DeGregory PR, Tsai YJ, Scida K, Richards I, Crooks RM. Quantitative electrochemical metalloimmunoassay for TFF3 in urine using a paper analytical device. *Analyst.* 2016;141(5):1734–44.
24. Li L, Wang T, Zhang Y, Xu C, Zhang L, Cheng X, Liu H, Chen X, Yu J. Editable TiO₂ nanomaterial-modified paper in situ for highly efficient detection of carcinoembryonic antigen by photoelectrochemical method. *ACS Appl Mater Interfaces.* 2018;10(17):14594–601.
25. Liu S, Zhao S, Tu W, Wang X, Wang X, Bao J, Wang Y, Han M, Dai Z. A signal on photoelectrochemical biosensor based on bismuth @N, O-codoped carbon core-shell nanohybrids for ultrasensitive detection of telomerase in HeLa cells. *Chem Eur J.* 2018;24(15):3677–82.
26. Liu Y, Yan K, Zhang J. Graphitic carbon nitride sensitized with CdS quantum dots for visible-light-driven photoelectrochemical aptasensing of tetracycline. *ACS Appl Mater Interfaces.* 2016;8(42):28255–64.
27. Dong YX, Cao JT, Wang B, Ma SH, Liu YM. Exciton–plasmon interactions between CdS@g-C₃N₄ heterojunction and Au@Ag nanoparticles coupled with DNAase-triggered signal amplification: toward highly sensitive photoelectrochemical bioanalysis of MicroRNA. *ACS Sustain Chem Eng.* 2017;5(11):10840–8.
28. Hou JY, Dong J, Zhu H, Teng X, Ai SY, Mang M. A simple and sensitive fluorescent sensor for methyl parathion based on L-tyrosine methyl ester functionalized carbon dots. *Biosens Bioelectron.* 2015;68:20–6.
29. Wang N, Fan H, Sun J, Han ZW, Dong J, Ai SY. Fluorine-doped carbon nitride quantum dots: ethylene glycol-assisted synthesis, fluorescent properties, and their application for bacterial imaging. *Carbon.* 2016;109:141–8.
30. Zeng XX, Tu WW, Li J, Bao JC, Dai ZH. Photoelectrochemical biosensor using enzyme-catalyzed in situ propagation of CdS quantum dots on graphene oxide. *ACS Appl Mater Interfaces.* 2014;6(18):16197–203.
31. Chen W, Fang J, Zhang Y, Chen G, Zhao S, Zhang C, Xu R, Bao J, Zhou Y, Xiang X. CdS nanosphere-decorated hollow polyhedral ZCO derived from a metal-organic framework (MOF) for effective photocatalytic water evolution. *Nanoscale.* 2018;10(9):4463–74.
32. Yang X, Li H, Zhang W, Sun M, Li L, Xu N, Wu J, Sun J. High visible photoelectrochemical activity of Ag nanoparticle-sandwiched CdS/Ag/ZnO nanorods. *ACS Appl Mater Interfaces.* 2017;9(1):658–67.
33. Zhang Z, Wang H, Chen Z, Wang X, Choo J, Chen LX. Plasmonic colorimetric sensors based on etching and growth of noble metal nanoparticles: strategies and applications. *Biosens Bioelectron.* 2018;114:52–65.
34. Jiang R, Li B, Fang C, Wang J. Metal/semiconductor hybrid nanostructures for plasmon-enhanced applications. *Adv Mater.* 2014;26:5274–309.
35. Zhang X, Zhu Y, Yang X, Wang S, Shen J, Lin B, Li C. Enhanced visible light photocatalytic activity of interlayer-isolated triplex Ag@SiO₂@TiO₂ core-shell nanoparticles. *Nanoscale.* 2013;5(8):3359–66.
36. Yao C, Wang W, Wang P, Zhao M, Li X, Zhang F. Near-infrared upconversion mesoporous cerium oxide hollow biophotocatalyst for concurrent pH-/H₂O₂-responsive O₂-evolving synergetic cancer therapy. *Adv Mater.* 2018;30(7):1704833.
37. Lance Kelly ECK, Zhao LL, Schatz GC. The optical properties of metal nanoparticles: the influence of size, shape, and dielectric environment. *J Phys Chem B.* 2003;107:668–77.
38. Chen B, Jiao X, Chen D. Size-controlled and size-designed synthesis of nano/submicrometer Ag particles. *Crystal Growth Des.* 2010;10(8):3378–86.
39. Zhang X, Liu Y, Kang Z. 3D branched ZnO nanowire arrays decorated with plasmonic Au nanoparticles for high-performance photoelectrochemical water splitting. *ACS Appl Mater Interfaces.* 2014;6(6):4480–9.
40. Tian Y, Tatsuma T. Mechanisms and applications of plasmon-induced charge separation at TiO₂ films loaded with gold nanoparticles. *J Am Chem Soc.* 2005;127(20):7632–7.
41. Chen HM, Chen C, Cheng LC, Wu PC, Cheng BH, Ho YZ, Tseng ML, Hsu YY, Chan TS, Lee JF, Liu RS, Tsai DP. Plasmon inducing effects for enhanced photoelectrochemical water splitting: X-ray absorption approach to electronic structures. *ACS Nano.* 2005;127(20):7632–7.

42. Shen Q, Zhao X, Zhou S, Hou W, Zhu JJ. ZnO/CdS hierarchical nanospheres for photoelectrochemical sensing of Cu^{2+} . *J Phys Chem C*. 2011;115(36):17958–64.
43. Zhang J, Xu X, Yuan Y, Yang C, Yang X. A Cu@Au nanoparticle-based colorimetric competition assay for the detection of sulfide anion and cysteine. *ACS Appl Mater Interfaces*. 2011;3(8):2928–31.
44. Ma Y, Su H, Kuang X, Li X, Zhang T, Tang B. Heterogeneous nano metal-organic framework fluorescence probe for highly selective and sensitive detection of hydrogen sulfide in living cells. *Anal Chem*. 2014;86(22):11459–63.
45. Ding L, Ma C, Li L, Zhang L, Yu J. A photoelectrochemical sensor for hydrogen sulfide in cancer cells based on the covalently and in situ grafting of CdS nanoparticles onto TiO_2 nanotubes. *J Electroanal Chem*. 2016;783:176–81.
46. Mao GJ, Wei TT, Wang XX, Huan SY, Lu DQ, Zhang J, Zhang XB, Tan W, Shen GL, Yu RQ. High-sensitivity naphthalene-based two-photon fluorescent probe suitable for direct bioimaging of H_2S in living cells. *Anal Chem*. 2013;85(16):7875–81.